

## 3D QSAR studies on a series of potent and high selective inhibitors for three kinases of RTK family

Hongyu Cao<sup>b</sup>, Huabei Zhang<sup>a,\*</sup>, Xuefang Zheng<sup>b,\*\*</sup>, Dabin Gao<sup>b</sup>

<sup>a</sup> Key Laboratory of Radiopharmaceuticals of Ministry of Education, College of Chemistry, Beijing Normal University, Beijing 100875, China

<sup>b</sup> Liaoning Key Laboratory of Bio-organic Chemistry, Dalian University, Dalian 116622, China

Received 11 June 2006; received in revised form 30 November 2006; accepted 1 December 2006

Available online 8 December 2006

### Abstract

For targets belonging to the same family of receptors, inhibitors often act at more than one biological target and produce a synergistic effect. Separate CoMFA and CoMSIA models were developed from our data set for the KDR, cKit and Tie-2 inhibitors. These models showed excellent internal predictability and consistency, and validation using test-set compounds yielded a good predictive power for the pIC<sub>50</sub> value. The field contour maps (CoMFA and CoMSIA) corresponding to the KDR, cKit and Tie-2 kinase subtypes reflected the characteristic similarities and differences between these types. These maps provided valuable information to facilitate structural modifications of the inhibitor to increase selectivity for the KDR over cKit and Tie-2.

© 2007 Elsevier Inc. All rights reserved.

**Keywords:** KDR; cKit; Tie-2; CoMFA; CoMSIA; Selective inhibitor

### 1. Introduction

Receptor tyrosine kinases (RTKs) are believed to play critical roles in signal transduction in a number of cellular functions and have been implicated in a variety of pathological conditions including angiogenesis cancer, tumor growth, atherosclerosis, diabetic, retinopathy, and inflammatory disease [1–5]. Vascular endothelial growth factor receptor (VEGFR) tyrosine kinase appears to be one of the most important mediators of physiological and pathological angiogenesis and is specifically expressed in vascular endothelial cells including VEGFR1 (Flt1) and KDR (VEGFR2) [6–8]. The activation of the VEGFR family RTKs and of the kinase insert domain-containing receptor tyrosine kinase (KDR) by vascular endothelial growth factors (VEGFs) is a potent regulator of vascular endothelial cells and has been directly linked to tumor angiogenesis and blood vessel-dependent metastasis [9–11]. KDR has also been shown to promote the production of

immature dendritic cell colonies via its kinase activity [12]. The cKit, one stem cell factor (SCF) receptor belonging to the RTK family, initiates cell growth and proliferation signal transduction cascades in response to stem cell factor binding [13]. The receptor tyrosine kinase, Tie-2, is expressed almost exclusively in endothelial cells [9,14]. The inhibition of Tie-2 with a soluble extracellular domain protein blocks tumor growth angiogenesis and metastasis [15–17]. VEGFRs play an early role in the differentiation of mesodermal cells into endothelial cells and the proliferation and migration of endothelial cells to form primitive tubular vessels [18–20]. These Tie RTKs are also involved in the later stages of modulating cell–cell and cell–matrix interaction [21–23]. The kinase activity of cKit is tightly regulated throughout its signaling cycle [13].

Often the biological targets belonging to the same family of receptors raise the problem of selectivity in receptor–ligand binding. Special efforts to design multiple activating drugs can be successfully made using computational methods to support biochemical studies and to design selective ligands for receptor subtypes.

Comparative molecular field analysis (CoMFA) [24] and comparative molecular similarity indices analysis (CoMSIA) [25] are two commonly used 3D QSAR methodologies that have been employed to recognize pharmacophoric units. The

\* Corresponding author. Tel.: +86 10 62207773; fax: +86 10 62200567.

\*\* Corresponding author.

E-mail addresses: [hbzhang@bnu.edu.cn](mailto:hbzhang@bnu.edu.cn) (H. Zhang),  
[dlxfzheng@163.com](mailto:dlxfzheng@163.com) (X. Zheng).

CoMFA method calculates the energies of steric and electrostatic interactions between the compound and the probe atom at the various intersections of a regular 3D lattice according to Lennard-Jones and Coulomb potentials. The resulting energies derived from these two potential functions can then be contoured to give a quantitative spatial description of the molecular properties. CoMSIA introduces the Gaussian function for the distance dependence between the molecular atoms and the probe atom in order to avoid some of the inherent deficiencies arising from the Lennard-Jones and Coulomb potential functional forms. CoMSIA is applied to gain insight into how steric, electrostatic, hydrophobic and hydrogen bonding interactions influence the activity of inhibitors. Partial least squares (PLS) is one of several techniques producing a QSAR equation to describe or predict differences in the values in one or more table columns from differences in other table columns [26]. The biological activity values of three different sets are related to the values of these interaction energies via PLS statistical models. And the greatest values of these coefficients can be mapped to the appropriate grid nodes to form a representation of some fields, which are displayed in some color [27]. As the main aim is to acquire the information to design selectivity inhibitors for three kinases of the RTK family, the PLS method performed with the assumptions of applying the same conformation and alignment would make the differences more explicit and available.

In order to understand the influence of different physico-chemical and structural parameters on inhibitor activity, 3D QSAR studies have been carried out in this paper. By the differences of the structural requirements for ligand binding to three kinase receptor subtypes, these models would offer utility in guiding the rational design of potent and selective KDR, cKit and Tie-2 inhibitors for therapeutic applications.

## 2. Material and methods

### 2.1. Data set

The present study was based on two fundamental assumptions. First, all of the inhibitors bind in the same fashion with three different kinases of the RTK family. The conformations of the compounds bound to the different kinases might be different. In our opinion, however, the assumption here is available when we take the lowest energy conformation as the active conformation. Second, data from different sources are available in our data set. Discarding inactive compounds and compounds with unspecified inhibitory activity, a data set composed of 71 KDR inhibitors was taken from two published papers. The activity values,  $IC_{50}$ , of these KDR inhibitors have been reported previously [28,29] and the  $pIC_{50}$  ( $-\log IC_{50}$ ) activity values are calculated and shown in Table 1. The total set is randomly divided into two subsets: a training set of 57 compounds for generating 3D QSAR models and a test set of 14 compounds for validating the quality of the models. Two additional data sets are also available: 39 compounds with inhibitory activities of cKit and 50 compounds with inhibitory activities of Tie-2 are also reported as  $IC_{50}$  values [29]. We

randomly divided these data sets into two subsets. The total set of cKit inhibitors (39 compounds) was divided into a training set of 32 inhibitors and a test set of 7 inhibitors while all the Tie-2 inhibitors (50 compounds) were divided into a training set of 41 compounds and the remaining compounds were assigned to the test set.

### 2.2. Molecular structures

A suitable conformation for the receptor is important in providing a realistic pharmacophore for 3D QSAR model building. Thus, the X-ray crystal structure of KDR kinase 1YWN was selected from the Protein Data Bank (PDB, <http://www.rcsb.org/pdb>) because it contains a co-crystallized ligand that is contained in our data set and this ligand is structurally most similar to the other compounds in our inhibitor set.

The 3D structure of the ligand (compound 69 in the data set) in 1YWN was extracted. After modifying atom types and adding hydrogen atoms with SYBYL7.0, an initial optimization of the structure was carried out using the TRIPOS force field with the Gasteiger–Hückel charges. Minimization was performed using the conjugated gradient method with a convergence criterion of 0.001 kcal/mol. All of the other molecules were constructed by modifying the side-chains of compound 69 using the Sketch module of the SYBYL software package. Following energy minimization, the side-chains of each structure were subjected to a systematic search routine of rotatable bonds in  $10^\circ$  increments from  $0^\circ$  to  $359^\circ$ . The energies of each conformation were computed and the lowest energy structures were used in alignment. The partial atomic charges required to estimate the electrostatic interaction were computed by semi-empirical molecular orbital methods using MOPAC with an AM1 Hamiltonian (keyword: NOMM).

### 2.3. Alignment procedure

A proper alignment of the structures is critical for obtaining valid 3D QSAR models. Furthermore, it is vital that all compounds are aligned in a pharmacological active orientation since the 3D QSAR model assumes that each structure exhibits activity at the same binding site of the receptor. To obtain a consistent alignment, compound 69 was selected as the template for the molecular alignment because it exhibits high affinity for KDR. The alignment moiety here was the rigid core and the common structure of each molecule (Fig. 1). An

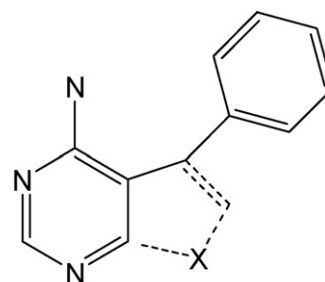


Fig. 1. The core used for common structure based alignment.

Table 1

Molecular structure and inhibitory activities (pIC<sub>50</sub>) for different kinases

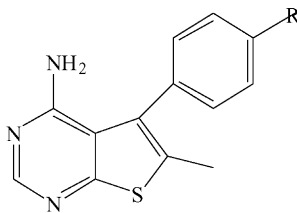
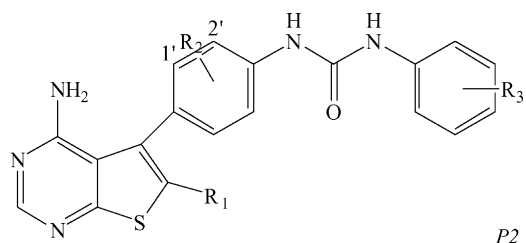
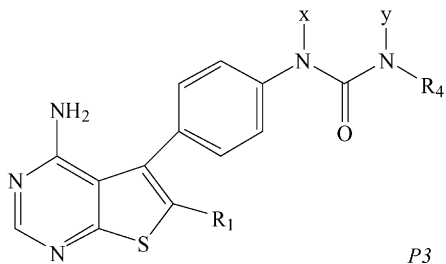
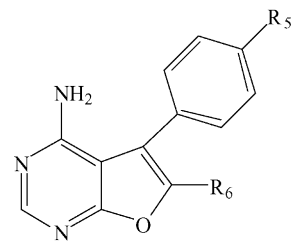
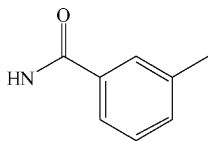
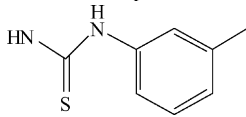
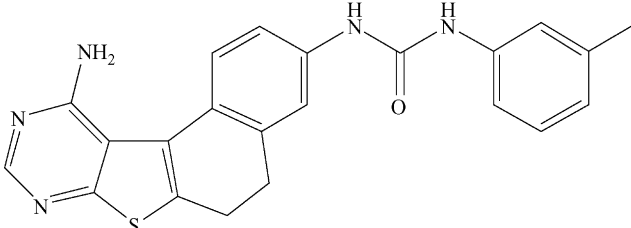
						
<i>P1</i>	<i>P2</i>					
						
<i>P3</i>	<i>P4</i>					
P1	R	KDR	R	KDR		
1	NH <sub>2</sub>	5.34	4	5.96		
2		5.34	5	6.77		
3		5.55	6*	6.12		
P2	R1	R2	R3	KDR	cKit	Tie-2
7*	CH <sub>3</sub>	H	H	7.44	7.49	5.92
8	CH <sub>3</sub>	H	2-CH <sub>3</sub>	6.59	7.17	5.89
9*	CH <sub>3</sub>	H	3-CH <sub>3</sub>	8.22	8.05	6.96
10 <sup>Δ</sup>	CH <sub>3</sub>	H	4-CH <sub>3</sub>	7.28	7.08	6.05
11	CH <sub>3</sub>	H	2-OCH <sub>3</sub>	6.96	7.30	6.04
12 <sup>Δ</sup>	CH <sub>3</sub>	H	3-OCH <sub>3</sub>	7.46	7.72	6.44
13 <sup>#</sup>	CH <sub>3</sub>	H	4-OCH <sub>3</sub>	7.16	7.82	5.80
14	CH <sub>3</sub>	H	2-F	6.96		6.00
15	CH <sub>3</sub>	H	3-F	7.26	7.57	6.40
16	CH <sub>3</sub>	H	4-F	7.28	7.48	6.07
17* <sup>#Δ</sup>	CH <sub>3</sub>	H	2-Cl	6.47	6.96	6.05
18	CH <sub>3</sub>	H	3-Cl	7.46	7.66	6.68
19	CH <sub>3</sub>	H	4-Cl	7.02	7.54	5.92
20	CH <sub>3</sub>	H	3-Br	7.34	7.30	6.89
21*	CH <sub>3</sub>	H	4-Br	6.92	7.32	5.96
22	CH <sub>3</sub>	H	3-CF <sub>3</sub>	7.28	6.85	7.00
23 <sup>Δ</sup>	CH <sub>3</sub>	H	3-CO <sub>2</sub> CH <sub>3</sub>	6.53	7.37	6.29
24	CH <sub>3</sub>	H	3,5-di-CH <sub>3</sub>	7.92	7.72	6.77
25	CH <sub>3</sub>	H	3,5-di-Cl	6.80	6.76	6.44
26 <sup>#</sup>	CH <sub>3</sub>	H	2-F-5-CF <sub>3</sub>	7.34	6.74	7.77
27	CH <sub>3</sub>	H	4-CF <sub>3</sub>	7.21		
28	CH <sub>3</sub>	H	2-F-5-CH <sub>3</sub>	7.47		
29*	(CH <sub>2</sub> ) <sub>2</sub> CONH <sub>2</sub>	H	3-CH <sub>3</sub>	7.77	6.80	6.92
30	(CH <sub>2</sub> ) <sub>2</sub> CONHCH <sub>3</sub>	H	3-CH <sub>3</sub>	6.48	6.40	6.33
31 <sup>#</sup>	(CH <sub>2</sub> ) <sub>2</sub> CON(CH <sub>3</sub> ) <sub>2</sub>	H	3-CH <sub>3</sub>	6.68	6.03	6.85

Table 1 (Continued)

P2	R1	R2	R3	KDR	cKit	Tie-2
32 <sup>Δ</sup>	CH <sub>2</sub> N-morpholinyl	H	3-CH <sub>3</sub>	6.68	6.24	6.37
33	CH <sub>2</sub> N-(4-CH <sub>3</sub> -piperazinyl)	H	3-CH <sub>3</sub>	6.23	6.10	6.20
34	CH <sub>2</sub> N(CH <sub>3</sub> ) <sub>2</sub>	H	3-CH <sub>3</sub>	6.74		
35	CH <sub>2</sub> CH <sub>3</sub>	H	3-CH <sub>3</sub>	7.58	7.55	6.47
36	H	H	3-CH <sub>3</sub>	8.52	8.22	6.14
37	<i>n</i> -Pr	H	3-CH <sub>3</sub>	7.58	7.09	6.54
38	<i>i</i> -Pr	H	3-CH <sub>3</sub>	6.89		6.24
39 <sup>Δ</sup>	Benzyl	H	3-CH <sub>3</sub>	6.55		6.06
40 <sup>#</sup>	CH <sub>2</sub> -pyridin-3-yl	H	3-CH <sub>3</sub>	7.47	6.10	6.60
41 <sup>*</sup>	CH <sub>2</sub> -pyridin-4-yl	H	3-CH <sub>3</sub>	7.28	6.02	6.57
42	CH <sub>2</sub> CH <sub>2</sub> OH	H	3-CH <sub>3</sub>	7.72	7.43	6.59
43 <sup>Δ</sup>	CH <sub>2</sub> CH <sub>2</sub> OCH <sub>3</sub>	H	3-CH <sub>3</sub>	7.19	6.44	6.66
44 <sup>#</sup>	(CH <sub>2</sub> ) <sub>3</sub> OH	H	3-CH <sub>3</sub>	7.82	7.59	6.96
45	CH <sub>2</sub> CH <sub>2</sub> N(CH <sub>3</sub> ) <sub>2</sub>	H	3-CH <sub>3</sub>	6.64	6.09	6.72
46 <sup>*</sup>	H	1'-F	3-CH <sub>3</sub>	7.96	7.57	
47	H	1'-Cl	3-CH <sub>3</sub>	7.00	6.70	
48	H	1'-OCH <sub>3</sub>	3-CH <sub>3</sub>	7.00	6.74	
49	H	2'-F	3-CH <sub>3</sub>	7.72	7.42	
50 <sup>#</sup>	H	2'-Cl	3-CH <sub>3</sub>	7.08	7.27	
51 <sup>*</sup>	H	2'-OCH <sub>3</sub>	3-CH <sub>3</sub>	7.89	7.55	
52	CH <sub>2</sub> CH <sub>3</sub>	H	3-CF <sub>3</sub>	7.30		
53	H	H	3-Cl	8.52		
P3	R1	R4	x	y	KDR	
54	CH <sub>3</sub>	Benzyl	H	H	6.48	
55	CH <sub>3</sub>	CH <sub>2</sub> -cyclohexyl	H	H	6.10	
56	CH <sub>3</sub>	3-Methylphenyl	CH <sub>3</sub>	H	7.26	
57	CH <sub>3</sub>	3-Methylphenyl	H	CH <sub>3</sub>	5.72	
58	CH <sub>2</sub> CH <sub>3</sub>	Cyclohexyl	H	H	6.77	
59 <sup>*</sup>	H	<i>n</i> -Bu	H	H	6.74	
60 <sup>*</sup>	H	<i>i</i> -Bu	H	H	5.77	
61					KDR	
					6.82	
P4	R5	R6	KDR		Tie-2	
62 <sup>*</sup>	4-OCH <sub>3</sub>	4-OCH <sub>3</sub> -phenyl	5.95		6.00	
63	4-N(CH <sub>3</sub> ) <sub>2</sub>	4-OCH <sub>3</sub> -phenyl	6.46		6.22	
64 <sup>Δ</sup>	4-OCH <sub>3</sub>	3-CONH <sub>2</sub> -phenyl	6.74		6.27	
65	4-OCH <sub>3</sub>	3-NHSO <sub>2</sub> CH <sub>3</sub> -phenyl	7.19		6.52	
66 <sup>*</sup>	4-OCH <sub>3</sub>	H	5.26			
67	4-Phenyl	3-NHSO <sub>2</sub> CH <sub>3</sub> -phenyl	7.44		6.72	
68	-NHCONH-phenyl	4-OCH <sub>3</sub> -phenyl	7.21		7.55	
69	-NHCONH-(2-fluoro-5-trifluoromethylphenyl)	4-OCH <sub>3</sub> -phenyl	8.52		8.70	
70 <sup>*</sup>	-NHCONH-cyclohexyl	4-OCH <sub>3</sub> -phenyl	6.73		7.23	
71	-NHCONH <sub>2</sub>	4-OCH <sub>3</sub> -phenyl	7.24		6.56	
72 <sup>Δ</sup>	4-OCH <sub>3</sub>	3,4-Dichlorophenyl			5.75	
73	4-OCH <sub>3</sub>	3-CON(CH <sub>3</sub> ) <sub>2</sub> -phenyl			5.83	
74	-NHCO-(3-fluorophenyl)	4-OCH <sub>3</sub> -phenyl			6.30	
75	-NHSO <sub>2</sub> -(3-chlorophenyl)	4-OCH <sub>3</sub> -phenyl			6.07	
76	-NHCONH-(4-chlorophenyl)	4-OCH <sub>3</sub> -phenyl			7.66	

Compounds marked with \*, # and <sup>Δ</sup> belong to the KDR, cKit and Tie-2 inhibitor test sets, respectively.

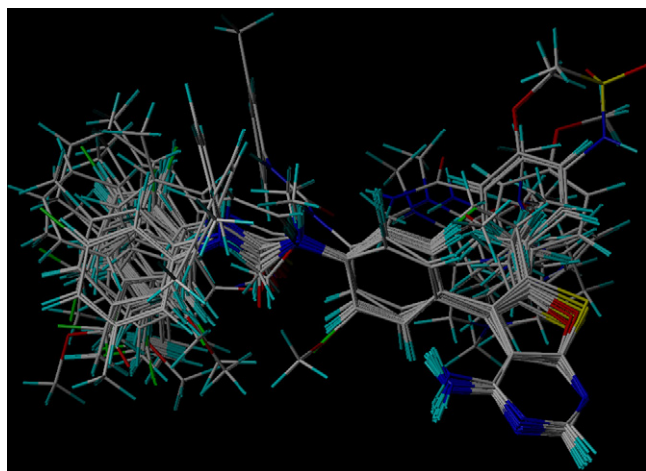


Fig. 2. Alignment of molecules using Align Database.

automatic alignment method was carried out by using Align Database. All of the molecules were inertially (grid orientation) aligned and put into a new database. Since the lowest energy conformation of compound 69 was used as the template and for other compounds the lowest energy conformations were chosen as the active conformations, the same aligned molecular database was used for building the models of cKit and Tie-2 inhibitors. The alignment of molecules was shown in Fig. 2 and the aligned molecules were provided as [Supplementary information](#).

#### 2.4. CoMFA and CoMSIA procedure

The standard CoMFA procedure, as implemented in SYBYL7.0, was performed. A 3D cubic lattice with a grid spacing of 2 Å was created automatically by the program to encompass all the aligned ligands.

A default  $sp^3$ -carbon probe atom with a van der Waals radius of 1.52 Å and a charge of +1.0 was used to generate steric (Lennard-Jones 6–12 potential) field energies and electrostatic (Coulombic potential) fields with a distance-dependent dielectric at each lattice point. The computed field energies were truncated to 30 kcal/mol for both steric and electrostatic fields.

In 1994, Klebe introduced the CoMSIA technique in which similarity indices are calculated at different points on a regularly spaced grid for pre-aligned molecules [25]. In this approach, five different similarity fields are calculated: steric, electrostatic, hydrophobic, hydrogen bond donor and hydrogen bond acceptor. These fields were selected to cover the major contributions to ligand binding. In CoMSIA fields, singularities were avoided at atomic positions because a Gaussian type distance dependence of each physicochemical property was adopted and thus no arbitrary cutoffs were necessary. The attenuation factor was set to the default value of 0.3.

#### 2.5. Partial least squares

To form the basis for a statistically significant model, a partial least squares regression was used to generate a linear

relationship that correlates changes in the computed fields with changes in the corresponding experimental values of the binding affinity ( $pIC_{50}$ ) for the data set of ligands. Biological activity values of these three sets of ligands were used as dependent variables in a PLS statistical analysis of all of the models. The column filtering value ( $\sigma$ ) was set to 2.0 kcal/mol to improve the signal-to-noise ratio by omitting those lattice points whose energy variations were below this threshold. Cross-validations were performed by the leave-one-out (LOO) procedure to determine the optimum number of components (ONC) and the coefficient  $q^2$ . Typically, whenever the increase in  $q^2$  with an additional component is less than 5%, the model with the fewer components is recommended over the model with the slightly higher  $q^2$  [30]. The optimum number of components obtained is then used to derive the final QSAR model using all of the training set compounds with non-cross-validation and to obtain the conventional correlation coefficient ( $r^2$ ).

### 3. Results and discussion

#### 3.1. CoMFA models

The CoMFA models were built after model development and validation based on internal predictions of the training set and the external predictions of the test set. PLS analyses of the KDR inhibitor training set showed a high cross-validated  $q^2$  value of 0.683 using four principal components and non-cross-validated  $r^2$  value of 0.933. In comparison with the CoMFA models built for KDR inhibitors, the inhibitor models for cKit and Tie-2 are inferior in predictable ability with the cross-validation  $q^2$  value (0.644 and 0.608, respectively) and the non-cross-validation  $r^2$  value (0.859 and 0.950, respectively). The statistical parameters for the three CoMFA models developed are presented in Table 2. All of the parameters of these CoMFA models showed certain reliability and feasible predictability to help us design

Table 2  
Statistical parameter of CoMFA and CoMSIA models of training sets

	KDR		cKit		Tie-2	
	CoMFA	CoMSIA	CoMFA	CoMSIA	CoMFA	CoMSIA
$q^2$ <sup>a</sup>	0.683	0.528	0.644	0.554	0.608	0.523
ONC <sup>b</sup>	4	3	3	2	5	4
$r^2$ <sup>c</sup>	0.933	0.853	0.859	0.750	0.950	0.851
S.E. <sup>d</sup>	0.180	0.264	0.228	0.299	0.144	0.245
$F$ <sup>e</sup>	181.925	102.437	56.842	43.591	132.492	51.341
Field contribution						
Steric	0.580	0.132	0.678	0.208	0.529	0.138
Electrostatic	0.420	0.250	0.322	0.206	0.471	0.278
Hydrophobic		0.294		0.245		0.299
Donor		0.142		0.102		0.141
Acceptor		0.182		0.238		0.144

<sup>a</sup> Cross-validation correlation coefficient.

<sup>b</sup> The optimum number of components.

<sup>c</sup> Non-cross-validation correlation coefficient.

<sup>d</sup> Standard error of estimate.

<sup>e</sup>  $F$ -ratio.

Table 3

Comparison of actual and predicted  $\text{pIC}_{50}$  values of the test sets for the KDR, cKit and Tie-2 CoMFA models

KDR				cKit				Tie-2			
	Actual	Predicted	Residual		Actual	Predicted	Residual		Actual	Predicted	Residual
6	6.12	6.43	−0.31	13	7.82	7.36	0.46	10	6.05	6.00	0.05
7	7.44	6.89	0.55	17	6.96	7.40	−0.44	12	6.44	6.54	−0.10
9	8.22	7.91	0.31	26	6.74	7.46	−0.72	17	6.05	6.11	−0.06
17	6.47	6.84	−0.37	31	6.03	6.47	−0.44	23	6.29	6.92	−0.63
21	6.92	7.15	−0.23	40	6.1	6.27	−0.17	32	6.37	6.65	−0.28
29	7.77	7.74	0.03	44	7.58	6.73	0.85	39	6.05	6.561	−0.51
41	7.28	7.33	−0.05	50	7.27	7.48	−0.21	43	6.66	6.66	0.00
46	7.96	7.16	0.80					64	6.27	6.24	0.03
51	7.89	7.54	0.35					72	5.75	6.19	0.44
59	6.74	6.64	0.10								
60	5.77	6.45	−0.68								
62	5.95	6.33	−0.38								
66	5.26	6.23	−0.97								
70	6.73	7.18	−0.45								

new and high selectivity KDR inhibitors. From Table 3 we can see that all compounds in the three test sets yield a good predicted  $\text{pIC}_{50}$  within 1 log unit of the experimental value. Fig. 3 shows the actual versus predicted values from three CoMFA models for training and test sets.

### 3.2. CoMSIA models

In the present studies, all of the CoMSIA models obtained with PLS analyses comprised of steric, electrostatic, hydrophobic, hydrogen bond donor and hydrogen bond

acceptor fields exhibited significant  $q^2$  values and were used for the predictive performance on the test set. Using the default CoMSIA parameters and all of the compounds in the KDR inhibitor training set, we derived a model with a  $q^2$  value of 0.528 with three components. Comparing with the  $q^2$  value of 0.683 for the CoMFA, the CoMSIA model showed a much lower  $q^2$  value. However, the performance for the predication of the activities of the training set was still reliable with a predicted  $r^2$  value of 0.853. The CoMSIA models built from cKit and Tie-2 inhibitor training sets showed significance with the cross-validation values  $q^2$

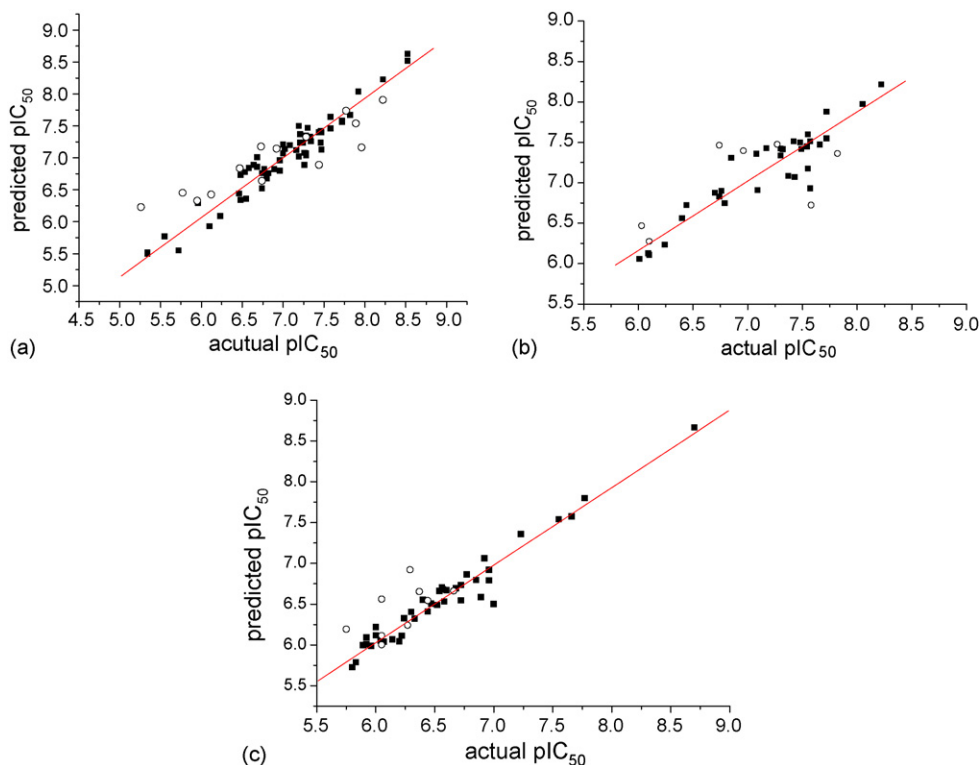


Fig. 3. Correlation between the actual and predicted activities of CoMFA models for the training set and test set. (a) KDR model; (b) cKit model; (c) Tie-2 model. (■) Compounds of the training set; (○) compounds of the test set.



(0.554 and 0.523, respectively), and non-cross-validation values  $r^2$  (0.750 and 0.851, respectively). All of the parameters obtained from the CoMSIA models are presented in Table 2.

### 3.3. Graphical interpretation of the results

The contour maps of CoMFA denote the region in the space where the aligned molecules would favorably or unfavorably interact with the receptor while the CoMSIA contour maps denote these areas within the specified region where the presence of a group with a particular physicochemical activity binds to the receptor. The CoMFA/CoMSIA results were graphically interpreted by field contribution maps using the 'STDEV  $\times$  COEFF' field type.

#### 3.3.1. CoMFA contour maps

Fig. 4(a–f) shows the contour maps derived from the CoMFA PLS model. The more potent analogue, compound 69, was embedded in the maps a, b, e and f while compound 35 was embedded in maps c and d to demonstrate its affinity for the steric and electrostatic regions of inhibitors. The areas of yellow indicate regions of steric hindrance to activity, while green areas indicate a steric contribution to potency. The blue regions indicate positive electrostatic charge potential associated with increased activity, while regions of red show negative charge with increased activity. All of the contours represented the default 80 and 20% level contributions for favored and disfavored regions, respectively, except Fig. 4(d) (represented 90 and 10% level contributions, respectively).

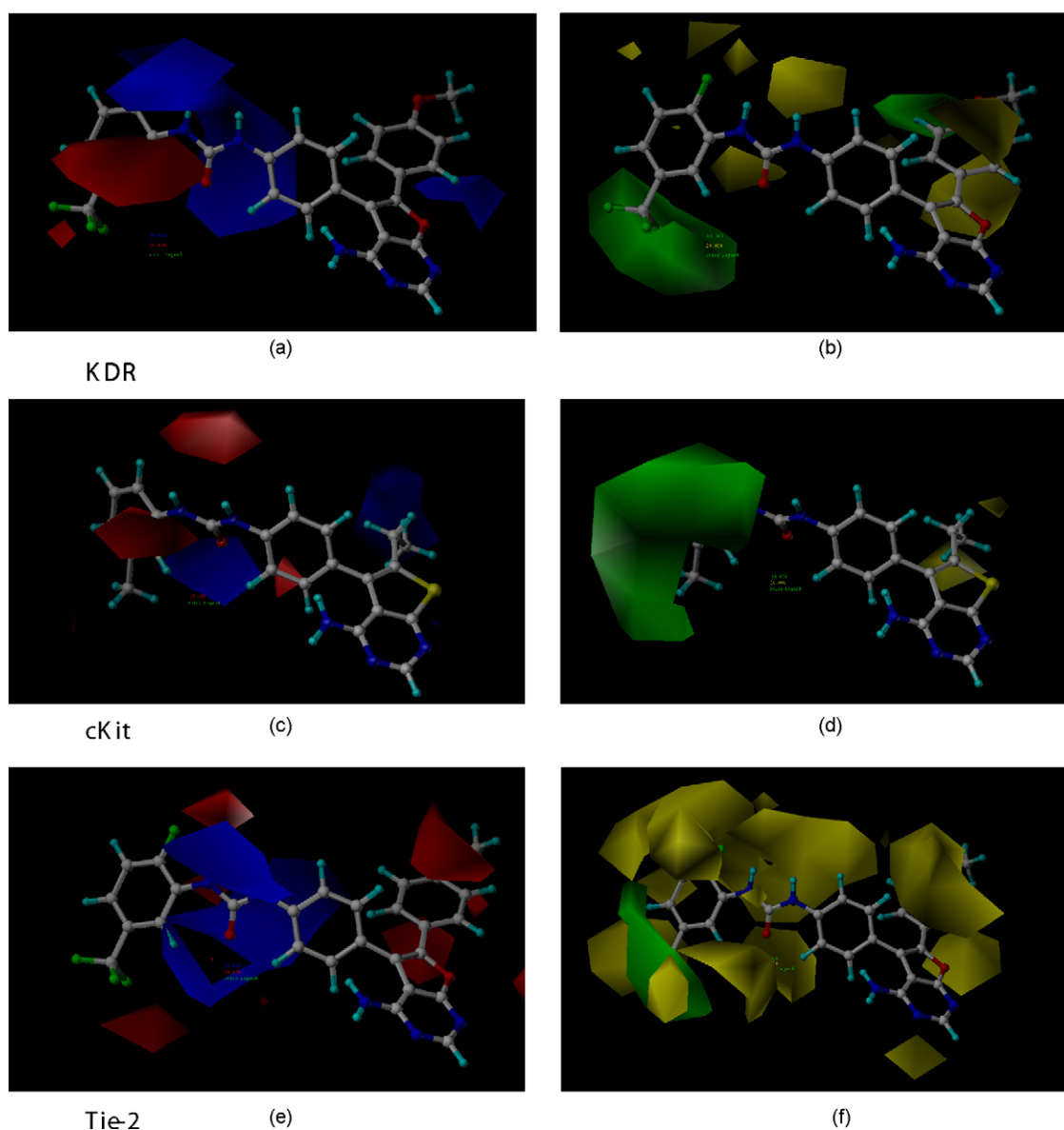


Fig. 4. The contour maps of CoMFA models for three receptors. (a, c and e) The CoMFA electrostatic field contour maps; red regions indicate the negative potential is favored, blue region shows that positive potential is favored; (b, d and f) the CoMFA steric field contour maps, sterically favored regions are in green; sterically disfavored regions are in yellow. Compound 69 was embedded in the maps a, b, e and f while compound 35 was embedded in the maps c and d.

Fig. 4 shows that the different physicochemical fields properties contours are mainly distributed within the region surrounding the diaryl urea unit and near the region enclosed by the 6-position of the thieno/furo [2,3-d]pyrimidines of the reference inhibitor. This suggests that these functional groups tune the affinity of each ligand. The yellow contour for the steric properties derived from the CoMFA studies indicate less steric interaction in the urea region and 6-positions of the thieno/fuopyrimidines. This will benefit the inhibitor for increasing the activity with the KDR receptor (Fig. 4(b)). As to electrostatic properties, the blue contour presented in the side of the diaryl urea unit region in the map suggests that positive electrostatic charge groups, e.g. the more positive charged nitrogen may favor enhanced affinity between KDR and its

inhibitors (Fig. 4(a)). The less bulky and positive substitution (e.g. positive charged nitrogen) on the 6-position of thieno/fuopyrimidine would increase the activity of KDR and cKit inhibitors while the negative substitution (e.g. functions containing fluorine or oxygen) is favored for Tie-2 of inhibitors. Less bulky and positive functions surrounding the urea moiety would benefit the activity of Tie-2 inhibitors.

The contributions from the steric and electrostatic fields for the present models are 0.580/0.420, 0.678/0.322 and 0.529/0.471 (Table 2), respectively, for the KDR, cKit and Tie-2 CoMFA models. Such contributions of field indicated that the variations in binding affinity among these inhibitors are dominated by steric interactions but distributed in different proportions across the binding sites of each of the three kinases

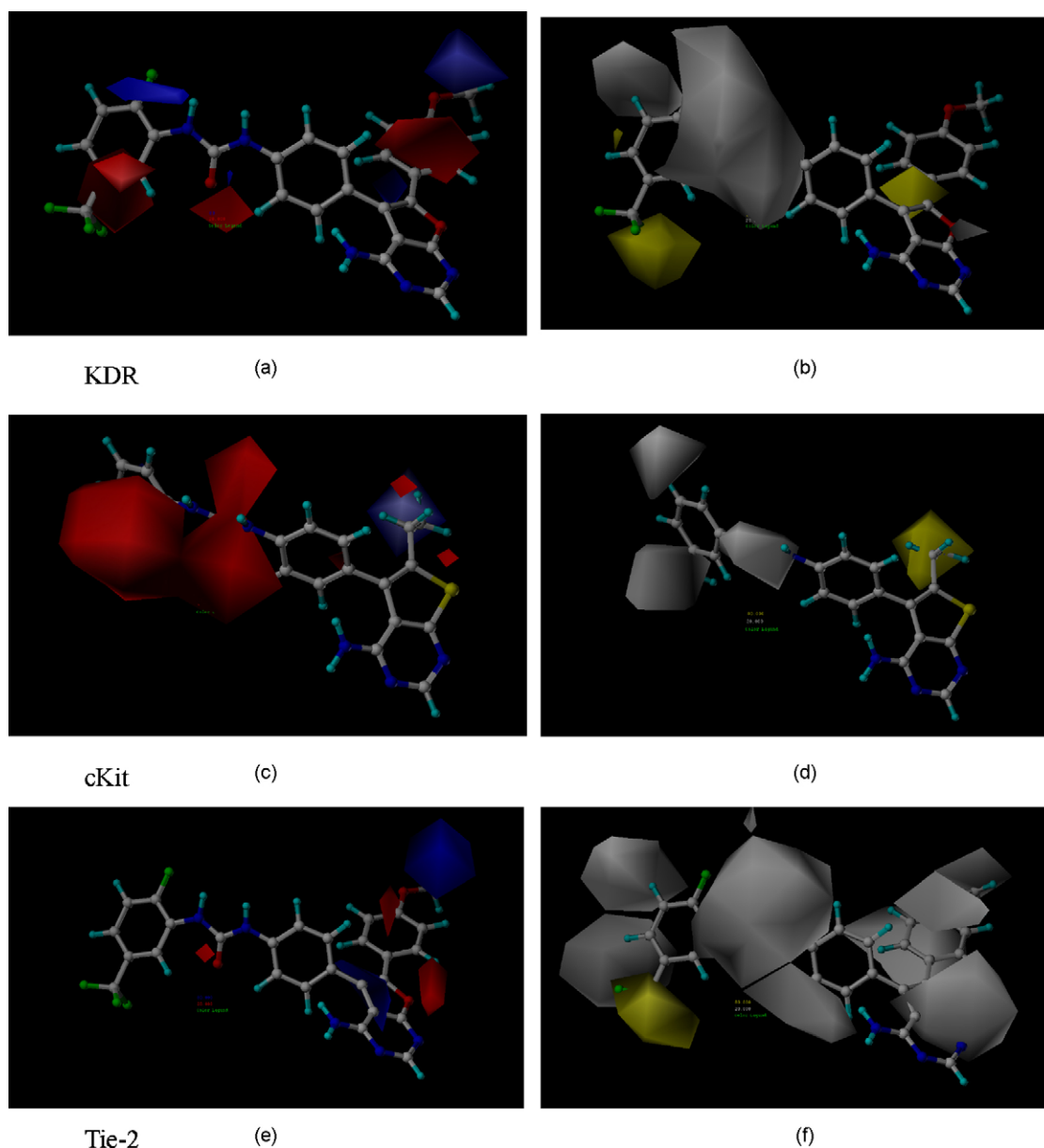


Fig. 5. The contour maps of CoMSIA models for three receptors. (a, c and e) The electrostatic field contour maps, red regions indicate disfavored areas of positive potential, blue regions indicate favored areas of positive potential; (b, d and f) the hydrophobic field contour maps. The yellow regions indicate favorable hydrophobic interactions and white regions indicate unfavorable hydrophobic interactions. Compound 69 was embedded in the maps a, b, e and f while compound 35 was embedded in the maps c and d.



receptors. This factor can be applied to design high potent and selective KDR inhibitors.

### 3.3.2. CoMSIA contour maps

Compared to standard CoMFA, the major advantage of CoMSIA is a better ability to visualize and interpret the obtained correlation in terms of the field contributions. Five contribution maps obtained by CoMSIA studies may be used to identify features important for interaction between small molecules and protein. The electrostatic and hydrophobic field contours of CoMSIA are presented in Fig. 5. Comparison of CoMSIA electrostatic maps indicates that the presence of a negative charge moiety in the urea phenyl region is crucial for cKit selectivity. Differences found in the region of the 6-positions of the thieno/fuopyrimidine units indicate that electronegative substitutions at this region will increase the selectivity for KDR over Tie-2 and cKit receptors. The red area presented at the urea phenyl of KDR contour maps indicates that pyridine substituent may be more favored than a phenyl urea substitution.

Table 2 shows that the hydrophobic field contributions for the three CoMSIA models show a higher contribution than other fields (0.294, 0.245 and 0.299, for the KDR, cKit and Tie-2 models, respectively). The yellow and white regions in Fig. 5 represent those areas of favorable and unfavorable hydrophobic interaction, respectively. The larger white regions at the 6-positions thieno/fuopyrimidine rings in Fig. 5(f) highlight the fact that hydrophobic substitutions will decrease the inhibitor affinity with Tie-2, while hydrophobic substitution in the same position favors KDR and cKit inhibition. The trifluoromethyl of compound 69 substituted by an aromatic function would be in accordance with the KDR hydrophobic field. Combined with the electrostatic and other field contour maps, reasonable structural modifications can be carried out to improve the activity and selectivity of KDR inhibitors.

The contributions of the five fields also show the differences of binding mode between inhibitors and three different receptors. The contributions of the steric field are 0.132 and 0.138 for KDR and Tie-2 CoMSIA models, respectively, while a high contribution is 0.208 for cKit CoMSIA model. The acceptor field contribution is 0.182 for KDR, which is lower than the value for kit (0.238) and higher than the value for Tie-2 (0.144). These parameters would alert us to increase the selectivity of inhibitors by changing this field contribution on the right position.

## 4. Conclusions

The development of RTK inhibitors is an active area of drug discovery research within the pharmaceutical industry. These 3D QSAR studies carried out combining CoMFA and CoMSIA have led to the identification of some of the important regions of the inhibitor that possess specific steric, hydrophobic, electronic and hydrogen bond interactions with three different kinases. The derived models explain the observed variance in the activity inhibitors which provides the basis for the design of new selective inhibitors of three RTK subtype receptors.

Different 3D QSAR models have been developed, KDR models, cKit models and Tie-2 models, to represent the molecular fields associated with the lead compounds acting at the KDR, cKit and Tie-2 receptors, respectively. An analysis of the model parameters and contour maps reveal the factors that influence the activity of those compounds for different receptors. Differences in requirements of different substitutions have been identified at position 6 of thieno/fuopyrimidine and urea moiety of inhibitors. This information is vital to steer the rational design of new drugs. For example, less bulky and electropositive substitutions in urea position and electronegative substitutions at the 6-position thieno/fuopyrimidine are predicted to increase the selectivity for the KDR receptor over the cKit and Tie-2 receptors. Based on the assumption of the same conformation and alignment, the differences in requirements of substitutions are more explicit and available. The 3D QSAR approach gives an insight into the different field contributions around the molecules and their influence on the overall activity. These 3D QSAR models provide valuable tools for guiding the rational design of novel inhibitors and for predicting their biological activity for the three RTK subtypes prior to chemical synthesis and biological testing.

## Acknowledgements

The authors are grateful to the Open Fund Support of the Liaoning Key Laboratory of Bio-organic Chemistry. This work was supported by the Natural Science Foundation of China (No.: 2021010) and Program for Liaoning Excellent Talents in University (No.: RC-04-10).

## Appendix A. Supplementary data

Supplementary data associated with this article can be found, in the online version, at [doi:10.1016/j.jmgm.2006.12.001](https://doi.org/10.1016/j.jmgm.2006.12.001).

## References

- [1] P. Carmeliet, R.K. Jain, Angiogenesis in cancer and other diseases, *Nature* 407 (2000) 249–257.
- [2] J. Folkman, Clinical applications of research on angiogenesis, *N. Engl. J. Med.* 333 (1995) 1757–1763.
- [3] J. Folkman, Angiogenesis in cancer, vascular, rheumatoid and other disease, *Nat. Med.* 1 (1995) 27–31.
- [4] B.R. Zetter, Angiogenesis and tumor metastasis, *Annu. Rev. Med.* 49 (1998) 407–424.
- [5] J.T. Kuethe, A. Wong, C.X. Qu, J. Smitrovich, I.W. Davies, D.L. Hughes, Synthesis of 5-substituted-1H-indol-2-yl-1H-quinolin-2-ones: a novel class of KDR kinase inhibitors, *J. Org. Chem.* 70 (2005) 2555–2567.
- [6] K.A. Thomas, Vascular endothelial growth factor, a potent and selective angiogenic agent, *J. Biol. Chem.* 271 (1996) 603–606.
- [7] B.I. Terman, M. Dougher-Vermazen, M.E. Carrion, D. Dimitrov, D.C. Armellino, D. Gospodarowicz, P. Bohlen, Identification of the KDR tyrosine kinase as a receptor for vascular endothelial cell growth factor, *Biochem. Biophys. Res. Commun.* 187 (3) (1992) 1579–1586.
- [8] C. De Vries, J.A. Escobedo, H. Ueno, K. Houck, N. Ferrara, L.T. Williams, The fms-like tyrosine kinase, a receptor for vascular endothelial growth factor, *Science* 255 (1992) 989–991.

- [9] G.D. Yancopoulos, S. Davis, N.W. Gale, J.S. Rudge, S.J. Wiegand, J. Holash, Vascular-specific growth factors and blood vessel formation, *Nature* 407 (2000) 242–248.
- [10] M.T. Bilodeau, M.E. Fraley, G.D. Hartman, Kinase insert domain-containing receptor kinase inhibitors as anti-angiogenic agents, *Expert Opin. Invest. Drugs* 11 (2002) 737–745.
- [11] M. Shibuya, L. Claesson-Welsh, Signal transduction by VEGF receptors in regulation of angiogenesis and lymphangiogenesis, *Exp. Cell Res.* 312 (2006) 549–560.
- [12] M.M. Dikov, J.E. Ohm, N. Ray, E.E. Tchekneva, J. Burlison, D. Moghannaki, S. Nadaf, D.P. Carbone, Differential roles of vascular endothelial growth factor receptors 1 and 2 in dendritic cell differentiation, *J. Immunol.* 174 (2005) 215–222.
- [13] C.D. Mol, D.R. Dougan, T.R. Schneider, R.J. Skene, M.L. Kraus, D.N. Scheibe, G.P. Snell, H. Zou, B.C. Sang, K.P. Wilson, Structural basis for the autoinhibition and STI-571 inhibition of c-Kit tyrosine kinase, *J. Biol. Chem.* 279 (2004) 31655–31663.
- [14] X.L. Niu, K.G. Peters, C.D. Kontos, Deletion of the carboxyl terminus of Tie2 enhances kinase activity, signaling, and function. Evidence for an autoinhibitory mechanism, *J. Biol. Chem.* 277 (2002) 31768–31773.
- [15] P.N. Lin, J.A. Buxton, A. Acheson, C. Radziejewski, P.C. Maisonpierre, K.G. Peters, Antiangiogenic gene therapy targeting the endothelium-specific receptor tyrosine kinase Tie2, *Proc. Natl. Acad. Sci. U.S.A.* 95 (1998) 8829–8834.
- [16] G. Siemeister, M. Schirner, K. Weindel, P. Reusch, A. Menrad, D. Marme, G. Martiny-Baron, Two independent mechanisms essential for tumor angiogenesis: inhibition of human melanoma xenograft growth by interfering with either the vascular endothelial growth factor receptor pathway or the Tie-2 pathway, *Cancer Res.* 59 (1999) 3185–3191.
- [17] P.N. Lin, P. Polverini, M. Dewhirst, S.Q. Shan, P.S. Rao, K. Peters, Inhibition of tumor angiogenesis using a soluble receptor establishes a role for Tie2 in pathologic vascular growth, *J. Clin. Invest.* 100 (1997) 2072–2078.
- [18] N. Ferrara, T. Davis-Smyth, The biology of vascular endothelial growth factor, *Endocr. Rev.* 18 (1997) 4–25.
- [19] P. Borgstrom, K.J. Hillan, P. Sriramaraio, N. Ferrara, Complete inhibition of angiogenesis and growth of microtumors by anti-vascular endothelial growth factor neutralizing antibody: novel concepts of angiostatic therapy from intravital video microscopy, *Cancer Res.* 56 (1996) 4032–4039.
- [20] A.P. Adamis, D.T. Shima, M.J. Tolentino, E.S. Gragoudas, N. Ferrara, J. Folkman, P.A. D'Amore, J.W. Miller, Inhibition of vascular endothelial growth factor prevents retinal ischemia-associated iris neovascularization in a nonhuman primate, *Arch. Ophthalmol.* 114 (1996) 66–71.
- [21] T.I. Koblizek, C. Weiss, G.D. Yancopoulos, U. Deutsch, W. Risau, Angiopoietin-1 induces sprouting angiogenesis in vitro, *Curr. Biol.* 8 (1998) 529–532.
- [22] B. Witzensbichler, P.C. Maisonpierre, P. Jones, G.D. Yancopoulos, J.M. Isner, Chemotactic properties of angiopoietin-1 and -2, ligands for the endothelial-specific receptor tyrosine kinase Tie2, *J. Biol. Chem.* 273 (1998) 18514–18521.
- [23] L.M. Shewchuk, A.M. Hassell, B. Ellis, W.D. Holmes, R. Davis, E.L. Horne, S.H. Kadwell, D.D. McKee, J.T. Moore, Structure of the Tie2 RTK domain self-inhibition by the nucleotide binding loop activation loop C-terminal tail, *Structure* 8 (2000) 1105–1113.
- [24] R.D. Cramer III, D.E. Patterson, J.D. Bunce, Comparative molecular field analysis (CoMFA) 1. Effect of shape on binding of steroids to carrier proteins, *J. Am. Chem. Soc.* 110 (1988) 5959–5967.
- [25] G. Klebe, U. Abraham, T. Mietzner, Molecular similarity indices in a comparative analysis (CoMSIA) of drug molecules to correlate and predict their biological activity, *J. Med. Chem.* 37 (1994) 4130–4146.
- [26] SYBYL 7.0 Manual, Tripos Inc., St. Louis, USA, 2004.
- [27] I.I. Baskin, I.G. Tikhonova, V.A. Palyulin, N.S. Zefirov, Selectivity fields: comparative molecular field analysis (CoMFA) of the glycine/NMDA and AMPA receptors, *J. Med. Chem.* 46 (2003) 4063–4069.
- [28] Y.J. Dai, Y. Guo, R.R. Frey, Z.Q. Ji, M.L. Curtin, A.A. Ahmed, D.H. Albert, L. Arnold, S.S. Arries, T. Barlozzari, J.L. Bauch, J.J. Bouska, P.F. Bousquet, G.A. Cunha, K.B. Glaser, J. Guo, J.L. Li, P.A. Marcotte, K.C. Marsh, M.D. Moskey, L.J. Pease, K.D. Stewart, V.S. Stoll, P. Tapang, N. Wishart, S.K. Davidsen, M.R. Michaelides, Thienopyrimidine ureas as novel and potent multitargeted receptor tyrosine kinase inhibitors, *J. Med. Chem.* 48 (2005) 6066–6083.
- [29] Y. Miyazaki, S. Matsunaga, J. Tang, Y. Maeda, M. Nakano, R.J. Philippe, M. Shibahara, W. Liu, H. Sato, L.P. Wang, R.T. Nolte, Novel 4-amino-furo[2,3-d]pyrimidines as Tie-2 and VEGFR2 dual inhibitors, *Bioorg. Med. Chem. Lett.* 15 (2005) 2203–2207.
- [30] U. Thibaut, G. Folkers, G. Klebe, H. Kubinyi, A. Merz, D. Rognan, Recommendations to CoMFA studies and 3D QSAR publications, in: H. Kubinyi (Ed.), *3D QSAR in Drug Design. Theory, Methods and Applications*, ESCOM, Leiden, The Netherlands, 1993, pp. 711–716.